Available online at www.sciencedirect.com

ScienceDirect

www.elsevier.com/locate/jes

JES JOURNAL OF ENVIRONMENTAL SCIENCES

www.jesc.ac.cn

Improvement of the activity and SO_2 tolerance of Sb-modified Mn/PG catalysts for NH_3-SCR at a low temperature

Xianlong Zhang[1,2,**], *Shuangshuang Lv*[1,**], *Xincheng Zhang*[1], *Kesong Xiao*[3], *Xueping Wu*[1,*]

[1] *School of Chemistry and Chemical Engineering, Hefei University of Technology, Hefei 230009, China*
[2] *Anhui Province Key Laboratory of Advanced Catalytic Materials and Reaction Engineering, Hefei University of Technology, Hefei 230009, China*
[3] *Instrumental Analysis Center, Hefei University of Technology, Hefei 230009, China*

ARTICLE INFO

Article history:
Received 14 November 2019
Revised 22 July 2020
Accepted 29 July 2020
Available online 21 August 2020

Keywords:
Manganese oxides
Antimony oxides
Low-temperature SCR
Metal sulfates
Sponge-like structure

ABSTRACT

A series of MnM/palygorskite (PG) (M = La, W, Mo, Sb, Mg) catalysts was prepared by the wetness co-impregnation method for low-temperature selective catalytic reduction (SCR) of NO with NH_3. Conversion efficiency followed the order Sb > Mo > La > W > Mg. A combination of various physico-chemical techniques was used to investigate the influence of Sb-modified Mn/PG catalysts. $MnSb_{0.156}$/PG catalyst showed highest NO conversion at low temperatures in the presence of SO_2 which reveals that addition of Sb oxides effectively enhances the SCR activity of catalysts. A SO_2 step-wise study showed that $MnSb_{0.156}$/PG catalyst displays higher durable resistance to SO_2 than Mn/PG catalyst, where the sulfating of active phase is greatly inhibited after Sb doping. Scanning electron microscopy and X-ray diffraction results showed that Sb loading enhances the dispersion of Mn oxides on the carrier surface. According to the results of characterization analyses, it is suggested that the main reason for the deactivation of Mn/PG is the formation of manganese sulfates which cause the permanent deactivation of Mn-based catalysts. For Sb-doped Mn/PG catalyst, SO_x ad-species formed were mainly combined with SbO_x rather than MnO_x. This preferential interaction between SbO_x and SO_2 effectively shields the MnO_x as active species from being sulfated by SO_2 resulting in the improvement of SO_2 tolerance on Sb-added catalyst. Multiple information support that, owing to the addition of Sb, original formed MnO_x crystallite has been completely transformed into highly dispersed amorphous phase accounting for higher SCR activity.

Introduction

Selective catalytic reduction (SCR) has been demonstrated as a feasible technology to reduce NO_x emission from stationary sources, including power plants and industrial boilers

* Corresponding author.
E-mail: xuepingw@ustc.edu.cn (X. Wu).
** These authors contributed equally to this work.

https://doi.org/10.1016/j.jes.2020.07.027
1001-0742/

(Burkardt and Weisweiler, 2001; Karami and Salehi, 2012). As the core technology of SCR, catalysts for SCR have caused extensive concern. Commercialised V_2O_5-WO_3 (MoO_3)/TiO_2 catalyst is widely used at 300–400°C, but this high temperature range requires SCR reactors to be located upstream of the particle removal device and desulphuriser to avoid reheating flue gas (Busca et al., 1998; Amiridis et al., 1999). However, the existences of high concentration of particles and other poison gas make the catalyst susceptible to deactivation. Therefore, developing a new candidate for SCR catalyst is important. And it has become essential to develop not only highly active catalysts at low-temperature but also materials for NO reduction resistant to catalytic deactivation.

NH_3-SCR catalysts work at relatively high NO_x at temperatures higher than 300°C over metal oxide catalyst (Topsøe, 1994; Rauch et al., 2015). However, high-temperature catalysts are expensive. Low-temperature (<300°C) NH_3-SCR catalysts are considered an ideal material for NO removal because of their energy efficiency. Many metal oxide catalysts have been applied to low-temperature NH_3-SCR, such as Mn/TiO_2 (Shi et al., 2013), V_2O_5/TiO_2 (Topsoe et al., 1995a), Cr/TiO_2 (Schneider et al., 1995), Cu/TiO_2 (Sreekanth et al., 2006). Amongst the low-temperature SCR catalysts, catalysts based on MnO_x have been proven to be the most active catalysts (Kim et al., 2010). Peña et al., 2004 compared various metal oxide-loaded catalysts and found that the activities of TiO_2-supported V, Cr, Fe, Mn, Ni, Co and Cu catalysts decrease according to the sequence of Mn > Cu > Cr > Co > Fe > V > Ni during low-temperature SCR of NO with NH_3. Qi and Yang (2003) found that Mn/TiO_2 catalysts are highly active for low-temperature SCR of NO with NH_3 with 100% NO conversion at 180°C (Zhang et al., 2015). Two types of catalysts based on MnO_x have been reported in the literature. One is the unloaded-MnO_x catalyst, which is prepared directly from different types of Mn precursors (Ettireddy et al., 2007); the other is the MnO_x-supported catalyst. The use of supports provides catalysts with high specific surface areas, good thermal stability and high dispersion of the active substance on surfaces. Supported-MnO_x catalyst is an excellent candidate for industrial use.

Various MnO_x-supported catalysts, such as MnO_x/TiO_2 (Lu et al., 2014; Zhang et al., 2011), MnO_x/Al_2O_3 (Aguero et al., 2009; Kapteijn et al., 1994b), MnO_x/CNT (carbon nanotube) (Wang et al., 2013; Zhang et al., 2013) and MnO_x/ACF (activated carbon fibre) (Sun et al., 2013; Marbán and Fuertes, 2001), have been reported. The use of support materials has been reported to play an important role in the activity of SCR catalysts (Jin et al., 2010b). In our previous study, a clay mineral, palygorskite (PG), was used as support instead of TiO_2 and Al_2O_3 to prepare a novel MnO_x-supported PG catalyst (MnO_x/PG); this support exhibited good performance and economy in low-temperature SCR of flue gas NO (Zhang et al., 2015).

Another critical issue in low-temperature NH_3-SCR catalyst is the sensitivity to S poisoning because S compounds can be formed over the catalyst in the presence of SO_2, leading to the loss of surface active sites and irreversible deactivation. The sensitivity of catalysts to SO_2 is an important consideration when the catalysts are operated in real flue gas for an extended period of time. Catalysts which are durably resistant to SO_2 have been found. Mn-Ce/TiO_2 catalyst demonstrates high resistance to SO_2 in flue gas at low temperatures (Jin et al., 2014). NO conversion over Mn/TiO_2 decreases from an initial value of 92% to 25% in 10 hr in the presence of 100 ppmV SO_2 at 150°C, whereas Mn-Ce/TiO_2 provides 60% NO conversion in 10 hr under the same conditions (Jin et al., 2014). Although the activity of Mn-Ce/TiO_2 in the presence of SO_2 was improved, the long-term stability of NO conversion was low and the concentration of SO_2 was only 100 ppmV SO_2. Therefore, developing a new catalyst which is durably resistant to SO_2 at a low temperature is important.

Some researchers have proposed addition of Sb to the catalyst to improve its tolerance to SO_2 poisoning. Results have shown that Sb improves the S resistance of the catalyst (Guo et al., 2016, Guo et al., 2018). Phil et al., 2008 found that Sb-doped V_2O_5/TiO_2 catalyst is best for low-temperature SO_2 deactivation resistance via a quantum chemical calculation study before experimentation. Du et al., 2012 reported that the SCR performance of V_2O_5/TiO_2 catalyst is enhanced when 1000 ppmV SO_2 is added to the feed stream with Sb and Nb. This active role may be due to the fact that the presence of SO_2 improves the SCR reaction to a certain degree.

In this work, the effect of adding Sb to Mn/PG for NH_3-SCR reaction is investigated. The influence of SO_2 on activities over Mn-$Sb_{0.156}$/PG is studied. Specific surface area (Brunauer-Emmett-Teller (BET)) analysis, scanning electron microscopy (SEM), X-ray diffraction (XRD) and X-ray photoelectron spectroscopy (XPS) were used to characterise the surface properties and crystalline structures of Sb-added catalysts. $SO_2 + O_2$ temperature-programmed desorption (TPD) analysis was employed to explore the poisoning mechanism of Sb-added catalysts. H_2-temperature-programmed reduction (TPR) analysis was applied to investigate the redox state of catalysts.

1. Materials and methods

1.1. Materials

The palygorskite, supplied by Xinzhou New Material factory (Anhui, China), was ground and 0.42–0.84 mm sieved. The chemical composition of the palygorskite was 69.44 wt.% SiO_2, 11.84 wt.% Al_2O_3, 5.14 wt.% Fe_2O_3, 12.16 wt.% MgO, 0.43 wt.% TiO_2, 0.5 wt.% K_2O, 0.21 wt.% CaO, and 0.28 wt.% others. All used chemicals including citric acid, manganese nitrate, antimony acetate, barium nitrate, cobalt nitrate and molybdenum nitrate were of analytical grade and purchased from Sinopharm Group Co., Ltd. Simulated flue gas provided by Nanjing Shangyuan Industrial Gas Plant.

1.2. Catalyst preparation

The wetness co-impregnation method with Mn nitrate and Sb acetate dissolved in citric acid is used to synthesize the $MnSb_y$/PG catalysts. $Mn(NO_3)_2$ (50 wt.%, 29.1 mmol) and $(CH_3COO)_3Sb$ (the molar ratio of Sb/Mn = 0.022–0.201, the loading of MnO_x was 8 wt.% based on PG) were dissolved in 2 mol/L citric acid solution as metal precursors. Ten gram of PG (0.42–0.84 mm) was added to this mixed solution and was impregnated for 24 hr. After dried at 50°C for 6 hr and 110°C for 12 hr, the samples were then calcined in air at 300°C for 3 hr

to obtain $MnSb_y$/PG catalyst (*y* represents the molar ratio of Sb to Mn in catalysts). Following the same procedure, a series of $MnM_{0.022}$/PG catalysts was prepared by using different metal (0.32 mmol La, W, Mo, Mg and Sb) precursor salts. All of the catalysts for evaluation were ground and sieved to 0.42–0.84 mm. The catalysts prepared were denoted as MnM_x/PG (*x* represents the molar ratio of M to Mn in catalysts).

1.3. *Catalytic activity measurements*

Catalytic activity tests for the reduction of NO by NH_3 were conducted in a fixed-bed quartz reactor containing 2 g of catalyst without any pre-treatment and operating under atmospheric pressure at 100–300°C. The feed gas mixture consisted of 600 ppmV of NH_3, 600 ppmV of NO, 3 vol.% O_2, 5 vol.% H_2O, 200 ppmV of SO_2 (when used) and Ar gas as the balance. The total flow rate of 350 mL/min was maintained for all tests and the gas hourly space velocity (GHSV) was approximately 5400 hr^{-1}. The concentrations of the gas inlet and outlet of NO_x (NO and NO_2) were measured online by a flue gas analyser (Testo350-XL, Testo AG, Germany), and the concentration of SO_2 was monitored by a SO_2 analyser (Testo300 M-I, Testo AG, Germany). Data were recorded when the reaction reached a steady state at each temperature for at least 1 hr. Catalyst performance was estimated by NO conversion calculated by the following equation:

$$X_{NO} = ([NO]_{in} - [NO]_{out})/[NO]_{in} \quad (1)$$

where X_{NO} represents the conversion of NO, $[NO]_{in}$ and $[NO]_{out}$ denote the inlet and outlet concentrations of NO, respectively.

1.4. *Catalyst characterisation*

Brunauer-Emmett-Teller (BET) surface area was measured from the N_2 adsorption and desorption isotherms at −196°C using the NOVA 2200e (Quantachrome, USA) adsorption analyser. Prior to analysis, 0.08–0.1 g of catalyst was preheated at 200°C for 4 hr under a N_2 atmosphere.

Scanning electron microscopy (SEM) images of the samples were obtained by a JSM-6490LV (Hitachi, Japan) analyser. Energy-dispersive X-ray spectroscopy (EDX) was used to determine the element content on the sample surface by a JSM-6490LV (Hitachi, Japan) analyser, EDX detector system operating at 20 kV and 80 mA.

X-ray diffraction (XRD) was performed on a D/MAx2500V diffractometer (Rigaku, Japan) equipped with a monochromated Cu $K\alpha$ radiation source. The catalysts were scanned at 2θ ranging from 10°−90°.

X-ray photoelectron spectroscopy (XPS) was used to explore the surface chemical properties of the tested catalyst, especially the state of the manganese species. Spectra were recorded on an ESCALAB250 (Thermo, USA) spectrometer using Al $K\alpha$ radiation (1486.6 eV). Binding energies (BE) were measured for Mn 2p, Sb 3d, O1s and S 2p.

SO_2 + O_2 temperature-programmed desorption (TPD) experiments were performed to specify the sulfate type in 1 g of SO_2-poisoned samples by a mass spectrometer (Hiden QGA, Beijing Hiden Analytical Technology Ltd, Germany). In a typical process, the catalysts (1 g) were pretreated at 120°C for 5 hr in Ar flow (350 mL/min). After cooled down to 50°C, the samples were initially reacted with 200 ppmV of SO_2-containing gases at 200°C for 2 hr. TPD experiments were subsequently performed by raising the temperature from 60 to 800°C at a heating rate of 5°C/min in Ar (350 mL/min) atmosphere.

H_2-temperature-programmed reduction (TPR) was conducted in an automated catalyst characterisation system. Prior to analysis, approximately 50 mg of the catalysts were pretreated at 50°C for 2 hr in ultra-high pure Ar (20 mL/min) steam. After preheating, the samples were tested by increasing the temperature from 50 to 800°C at a rate of 10°C/min under 5 vol.% H_2/Ar. The consumption of H_2 was detected by a mass spectrometer (Hiden QGA, Beijing Hiden Analytical Technology Ltd, Germany).

2. Results

2.1. *Activity studies*

2.1.1. *Influence of promoters on SCR activity without SO_2*

Fig. 1 shows the NO conversion in the SCR activity over different metal-promoted Mn/PG catalysts in the temperature range of 100–300°C. All catalysts showed increasing trend in NO conversion with temperature increased until 250°C (nearly 100%). Then, the NO conversion started to decrease for all catalysts except for $MnSb_{0.022}$/PG at temperature higher than 250°C. The low-temperature NO conversion of La, W, Mo, Mg and Sb-promoted Mn/PG catalysts followed the order Sb > Mo > La > W > Mg. Obviously, amongst all catalysts, Sb doped catalyst showed not only the best SCR activity, but also the widest operating-temperature windows. Park et al., 2001 reported that NH_3 are oxidised into NO and NO_2 at sufficiently high temperatures over a natural Mn ore catalyst in the presence of O_2; they attributed the decrease in NO conversion to NH_3 oxidation over the Mn ore catalyst. The decreases in NO conversion at high temperatures (> 250°C) for above catalysts (except for $MnSb_{0.22}$/PG) were the same as that for the reported Mn ore catalyst, indicating that the NH_3 oxidation was accelerated along with the increasing temperature. Comparatively, the Sb addition not only enhanced the SCR activity of catalysts at lower temperatures, but also inhibited the decrease in NO conversion at temperature higher than 250°C caused by the excessive oxidation of NH_3. What's more, the surface active manganese species might be formed in a different state from that on the original or other metal added catalysts.

2.1.2. *Effect of Sb loading on the tolerance of Mn/PG to SO_2*

NO conversion of Sb-modified Mn/PG catalysts ($MnSb_x$/PG) in the presence of SO_2 is shown in Fig. 2**a**. NO conversion for all catalysts presented the same tendency increased as temperature rose. It was found that the Sb loading content had moderate effect on catalytic performance. Compared to other samples, $MnSb_{0.156}$/PG showed the best performance especially at 125–250°C. According to this result, we followingly selected $MnSb_{0.156}$/PG as typical sample for the further study on the sulfur resistance of Sb loading. Comparing to the results in the absence of SO_2 displayed above, the NO conversion for Mn/PG was much lower in the whole temperature range, indicating a serious deactivation caused by SO_2. The difference

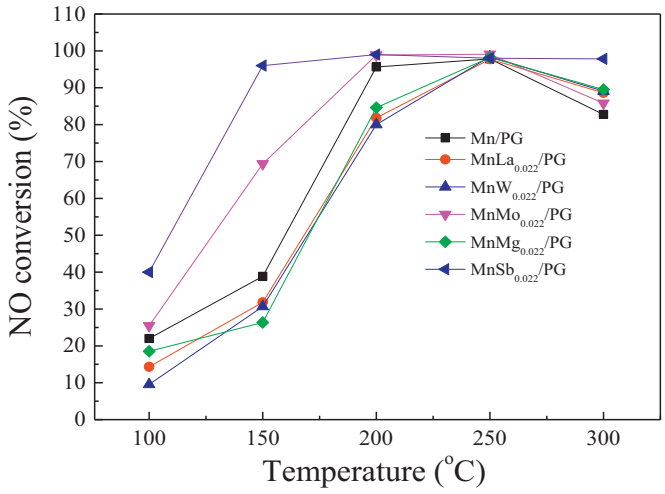

Fig. 1 – Effect of promoter loading on the Mn/palygorskite (PG) catalysts. Reaction conditions: [NO] = [NH_3] = 600 ppmV, [O_2] = 3 vol.%, [H_2O] = 5 vol.%, Ar gas as the balance and gas hourly space velocity (GHSV) = 5400 hr^{-1}. [X] refers to the concentration of the species X.

was that no obvious decrease in NO conversion is observed for Mn/PG catalyst at higher temperature, which was discussed in our previous study (Zhang et al., 2015). However, for Sb added catalysts ($MnSb_x$/PG), similar tendency in NO conversion were obtained as that for $MnSb_{0.22}$/PG showed in Fig. 1. Based on this point, it can be confirmed that a high SCR activity with reliable resistance to SO_2 poisoning can be achieved over Sb-added catalysts. Side reaction such as NO oxidation/NO_2 decomposition at high temperatures (i.e., > 400°C) could occur: $2NO + O_2 \leftrightarrow 2NO_2$, so outlet NO_2 concentration was much low in the temperature range of 100–300°C (Colombo et al., 2010; Schuler et al., 2009). We also detected outlet NO_2 concentration but found it was very low during the SCR process. Results in Fig. 2**b** illustrated the concentration of NO_2 with a negligible value less than 5 ppmV in the entire operating temperature range studied over. To explore the potential interaction of SbO_x and MnO_x answering for the significant promotion on the performance of the catalyst, the sole Sb-added sample ($Sb_{0.156}$/PG) was also prepared and estimated for SCR in the same conditions. $Sb_{0.156}$/PG was found to be inactive for SCR reaction with a negligible NO conversion, suggesting that Sb acts as an effective promoter other than an additional active specie.

For further evaluating the catalyst's tolerance to SO_2 contributed by doping of Sb, we calculated the decrease in NO conversion caused by SO_2 (200 ppmV) for Mn/PG and $MnSb_{0.156}$/PG, respectively, as shown in Fig. 2**c**. As can be seen, the presence of 200 ppmV gaseous SO_2 leads to the decreases in NO conversion for both of them, implying that the deactivation has happened. However, the deactivation on Mn/PG is much more serious than that of $MnSb_{0.156}$/PG especially in the temperatures range from 150 to 250°C. For example, at 200°C, the decrease in NO conversion for Mn/PG caused by SO_2 is nearly 60%, while just 1% decrease is obtained for Sb-added catalyst. It should be noted that the decrease in NO conversion for $MnSb_{0.156}$/PG during the entire temperature range is all less than 10%.

In comprehension, from the results of those activity studies, it can be deduced that the doping of Sb as additive not only promotes the SCR activity but also enhances the resistance to SO_2 poisoning. Accordingly, the synergistic action between Sb promoter and active Mn species could be expected.

2.1.3. *NO oxidation activity*

It was reported that the oxidation of NO to NO_2 may be a key step for NH_3-SCR over manganese based catalysts, which is easily inhibited by the presence of gaseous SO_2 (Li et al., 2012; Zhang et al., 2008). To investigate whether there was a direct relationship between the NO oxidation to NO_2 and the SCR activity, the behaviours of NO oxidation to NO_2 over the Mn/PG and $MnSb_{0.156}$/PG catalysts were evaluated and compared as shown in Fig. 3. Firstly, the conversion of NO to NO_2 slightly increased as temperature rose for both of the catalysts, but the tendency was quite inconsistent with that of SCR activity as illustrated in Fig. 1. Secondly, the NO to NO_2 conversion over the $MnSb_{0.156}$/PG catalyst was also moderately higher than that over Mn/PG catalyst. However, the increment in NO to NO_2 conversion contributed by the addition of Sb was less than 15%, which is negligible compared with that in NO conversion in SCR process. Based on the point, it is reasonable to deduce that the NO oxidation to NO_2 is inessential for SCR for both of those catalysts. Consequently, the great improvement in SCR activity and SO_2 tolerance should not be ascribed to the slightly promoting of NO oxidation to NO_2 over the Sb-added catalyst.

2.1.4. *SO_2 step-wise study*

According to Eley–Rideal mechanism model, and the experience on the performance of commercial V_2O_5-WO_3/TiO_2 catalyst, the deposition of ammonia sulfates was believed to be the main reason for the deactivation caused by SO_2 (Forzatti, 2001; Kobayashi and Hagi, 2006). However, for manganese based catalyst with excellent SCR activity at low temperatures, the deactivation caused by SO_2 is also a blank wall and the mechanism still remains controverted (Wu et al., 2009; Park et al.,

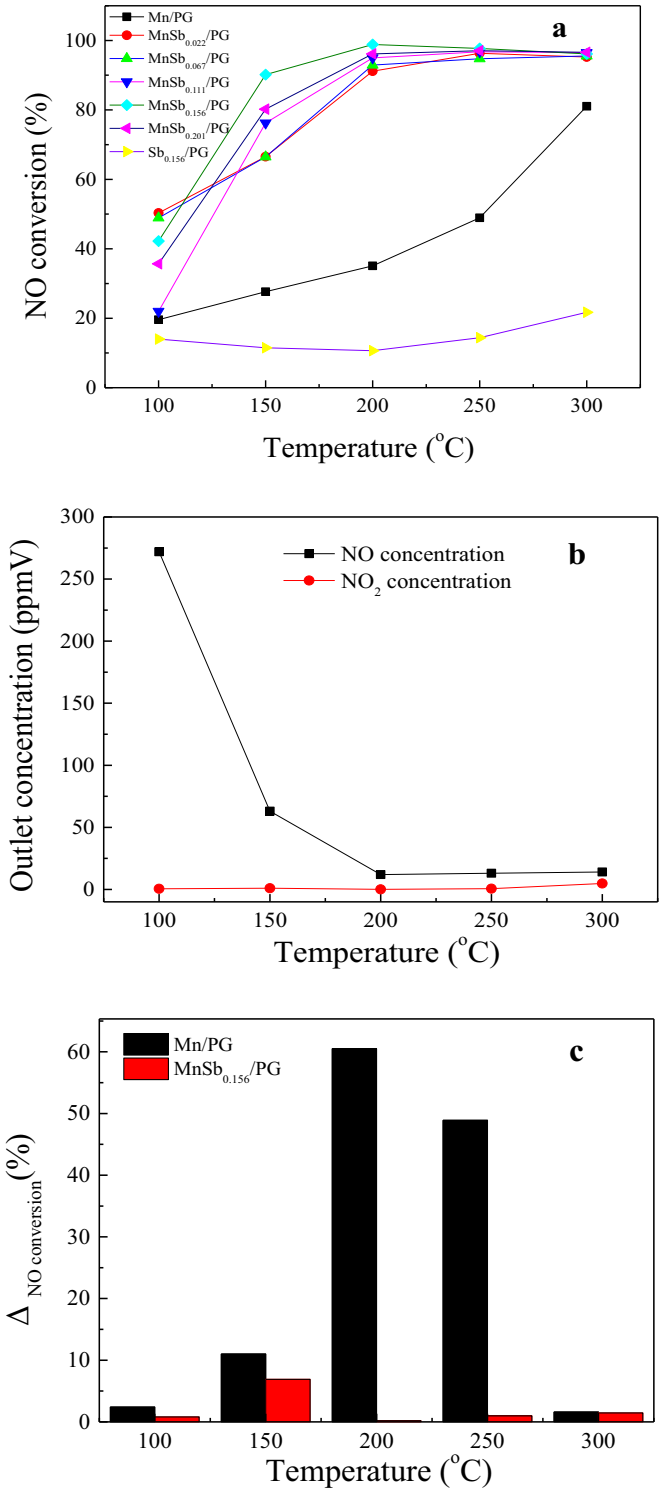

Fig. 2 – (a) Effect of Sb loading on NO conversion, (b) concentrations of NO and NO_2 on $MnSb_{0.156}$/PG, and (c) decrease in NO conversion ($\Delta_{NO\ conversion}$) caused by SO_2 (200 ppmV) for Mn/PG and $MnSb_{0.156}$/PG. Reaction conditions: [NO] = [NH_3] = 600 ppmV, [SO_2] = 200 ppmV, [O_2] = 3 vol.%, [H_2O] = 5 vol.%, Ar gas as the balance and GHSV = 5400 hr^{-1}.

2013; Jin et al., 2010a; Sheng et al., 2012). Generally, besides the deposition of ammonia sulfates, the formation of manganese sulfates was also considered to be a potential reason for the deactivation of manganese-based catalysts (Wu et al., 2009; Biervliet et al., 1998).

In this work, the SO_2 tolerance of Mn/PG and $MnSb_{0.156}$/PG catalysts was investigated via a step-wise of SO_2 durable steady SCR reaction. The SO_2 step-wise experiments were performed under isothermal conditions at 200°C. As illustrated in Fig. 4a, the SCR activities of NO with NH_3 over Mn/PG and

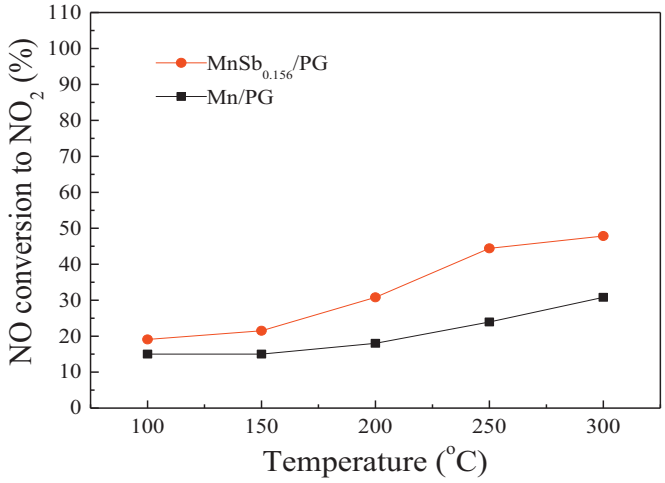

Fig. 3 – NO conversion to NO_2 for Mn/PG and $MnSb_{0.156}$/PG catalysts. Reaction conditions: [NO] = 600 ppmV, [O_2] = 3 vol.%, [H_2O] = 5 vol.%, Ar gas as the balance and GHSV = 5400 hr^{-1}.

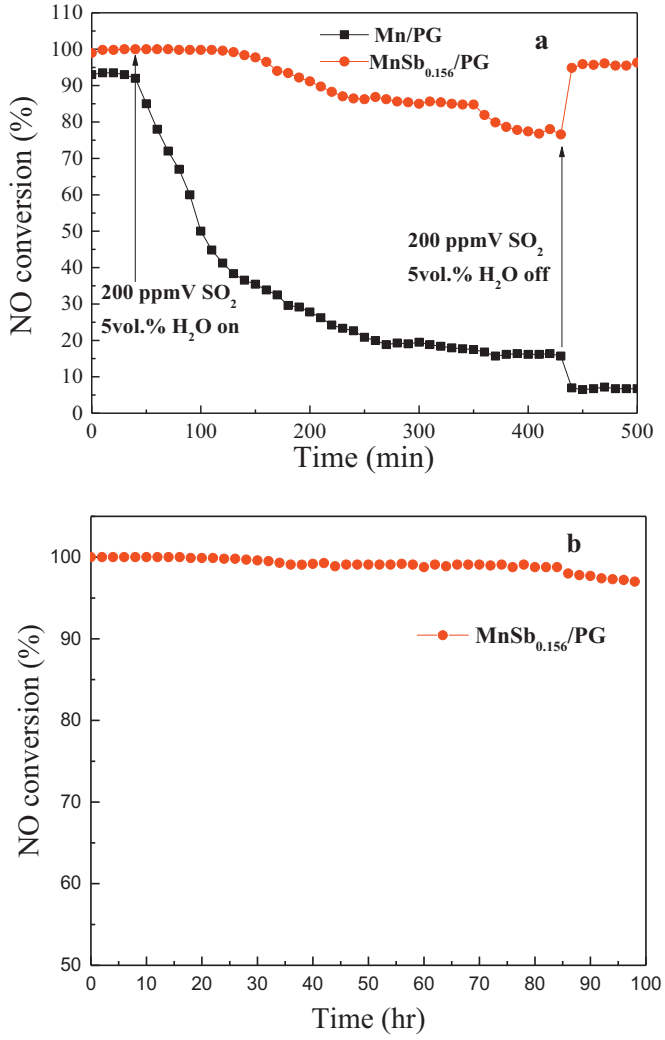

Fig. 4 – (a) Effect of SO_2 on NO conversion for Mn/PG and $MnSb_{0.156}$/PG catalysts. Reaction conditions: [NO] = [NH_3] = 600 ppmV, [SO_2] = 200 ppmV, [O_2] = 3 vol.%, [H_2O] = 5 vol.%, Ar gas as the balance and GHSV = 5400 hr^{-1}, T = 200 °C. (b) Stability of $MnSb_{0.156}$/PG catalysts. Reaction conditions: [NO] = [NH_3] = 600 ppmV, [O_2] = 3 vol.%, Ar gas as the balance and GHSV = 5400 hr^{-1}, T = 200 °C.

$MnSb_{0.156}$/PG catalysts were initially stable for 30 min in simulated flue gas without SO_2. After 200 ppmV of SO_2 was added to the simulated flue gas, NO conversion of Mn/PG catalyst decreased rapidly to lower than 20% within 400 min and could not be recovered after removal of SO_2. As a result, after the removal of SO_2 and H_2O from the flue gas, a little increase in indicating value of the outlet NO_x appeared leading to a decrease in calculated NO conversion. Because it did not interfere the result that an irreversible deactivation had happened on Mn/PG catalyst, we did not revise this deviation with respect for the facticity of experimental data. It was widely reported that there are two possible routes accounting for the deactivation of Mn based catalysts for SCR caused by SO_2. One was the deposition of ammonium sulfates ($(NH_4)_2SO_4$, NH_4HSO_4 or the mixture) which depend on a dynamic balance between the formation and decomposition of ammonium sulfates in SCR reactions (Yu et al., 2010). This problem could be resolved by rising the reaction temperature, because at high temperatures, the formation of ammonium sulfates could be inhibited and the decomposition accelerated. Otherwise, in the case of SO_2 being removed, the balance would move to the decomposition until all deposited ammonium sulfates being consumed. In other words, the deactivation of catalysts through this route could be recovered when SO_2 was removed from the flue gas. Another suggested route was the formation of manganese sulfates. It could not be decomposed at temperature lower than 800°C and is hard to participate in NH_3-SCR redox cycle reaction of electron, implying that this type of deactivation cannot be resolved in 100–300°C (Huang et al., 2003). Based on these analyses, it was reasonable to suggest that the deactivation of Mn/PG caused by SO_2 is mainly the sulfation of surface active species (MnO_x) (Shu et al., 2014). However, for Sb-added catalyst, the profile in NO conversion during SO_2 step-wise experience was quite different from that of Mn/PG. When SO_2 was introduced, NO conversion for $MnSb_{0.156}$/PG remained nearly 100% for a quite long time (about 120 min) followed by a mild decrease from 100% to a steady 78%. When SO_2 was removed from the feed gas, NO conversion was recovered immediately. This phenomenon could be due to the formation of ammonium sulfates ($(NH_4)_2SO_4$ or NH_4HSO_4) occurring slowly over Sb-added Mn/PG catalyst leading to a completely decomposition of ammonium sulfates after removal of SO_2. This result also confirmed that the sulfation of catalyst active sites (MnO_x) is greatly lessened after Sb doping during SCR reaction in the presence of SO_2, which may be the key reason for the great enhancement in SO_2 tolerance of the catalysts after Sb addition. Therefore, it can be deduced that the addition of Sb shields surface active species (MnO_x) from being sulfated but slightly boost the deposition of ammonium sulfates. As a result, $MnSb_{0.156}$/PG catalyst displays higher durable resistance to SO_2 than Mn/PG catalyst. In order to further explore whether the $MnSb_{0.156}$/PG catalysts had practical application value, a long-term stability test was carried out on the $MnSb_{0.156}$/PG catalysts under a GHSV of 5400 hr^{-1}. As shown in Fig. 4**b**, the initial NO conversion of the $MnSb_{0.156}$/PG catalysts was 100% at 200°C. After 96 hr, the NO conversion of the $MnSb_{0.156}$/PG catalysts decreased slightly to 96%. It was suggested the $MnSb_{0.156}$/PG catalysts had application potential.

2.2. *Catalytic characterisation*

2.2.1. *SEM analyses*

Fresh and used samples of Mn/PG and $MnSb_{0.156}$/PG were characterised by SEM to determine the morphologies of catalysts. As shown in Fig. 5, the characteristics of the catalyst's surface have changed due to the Sb loading. For fresh Mn/PG, the surface of the catalyst carrier was scattered with a layer of clear particles corresponding to the microlite of Mn oxides phase, and the fabric of PG carrier was not observed. In contrast, the micrographs of fresh $MnSb_{0.156}$/PG (Fig. 5**b**) were entirely different from that of Mn/PG. After modified by Sb, the visible micro-particles of Mn oxides completely disappeared and the fabric of PG clearly exposed with sponge like structure. This result indicated that addition of Sb oxides causes Mn oxides to become highly dispersed on the catalyst's surface, and the size of newly-formed material is close to ultra-manometer, which is beneficial to SCR of NO by NH_3. Firstly, It was more likely because the presence of Sb inhibited the crystallization of precursor of Mn specie ($Mn(NO_3)_2$) during the drying process. Secondly, the decomposition of Mn nitrate to form MnO_x specie was remarkably affected by the co-decomposition of $Sb(CH_3COO)_3$ during the calcination process. Apparently, a composite oxide of Mn and Sb had formed a better dispersion of active species and a special sponge-like structure. For used Mn/PG sample (for SCR in the presence of 200 ppmV SO_2), the boundary between surface particles became vague. It was more likely due to the aggregation and growth of those particles caused by the sulfation of manganese oxides. As a result, the surface layer of used Mn/PG catalyst was even denser than that of fresh catalyst. However, from the images of used $MnSb_{0.156}$/PG, no obvious difference from fresh $MnSb_{0.156}$/PG was found. The sponge like fabric of PG remained steady without accumulation of bulk compounds.

These results reveal that the sponge-like structure of $MnSb_{0.156}$/PG not only improves the dispersion of MnO_x on the catalyst surface but also inhibits the sulfation of manganese oxides, due to the transformation of manganese active species from micro-crystal to amorphous phase. Besides, the surface assembling of metal elements for each catalyst was also examined by energy dispersive spectroscope (EDS). The resultant peak intensities for the fresh and used catalysts are presented in Fig. 5**e-h**. For fresh catalysts, the intensity of Mn element on Mn/PG was found to be much higher than that on $MnSb_{0.156}$/PG, implying higher accumulation of manganese oxides on Mn/PG and better dispersion of manganese oxides on $MnSb_{0.156}$/PG, which is in accordance with the phenomena observed in SEM image. For used catalysts, the peak of Mn was found to be enhanced on Mn/PG but remained low on $MnSb_{0.156}$/PG. This information also supported that the accumulation of micro-particles caused by the sulfating of manganese species occurs on Mn/PG but avoids on $MnSb_{0.156}$/PG catalyst.

2.2.2. *XRD analyses*

The XRD patterns of the Sb-modified Mn/PG samples are shown in Fig. 6. All samples were calcined at 300°C to maintain the primary structure of PG. Several diffraction peaks observed at 14.2°, 16.4°, 20.3°, 21.3°, 35.4° and 61.8° matching the support PG well (Middea et al., 2015). While, the appearance

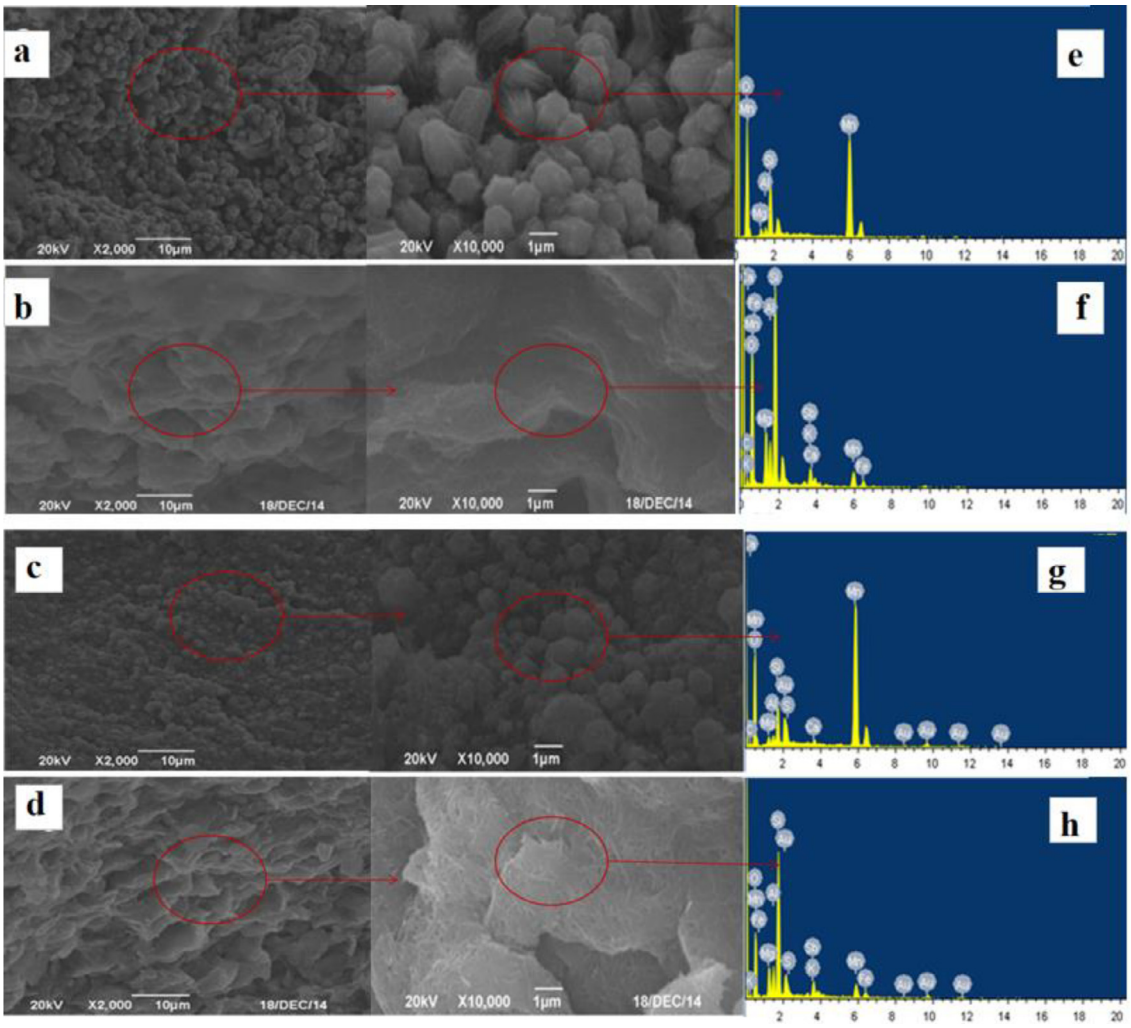

Fig. 5 – Scanning electron microscopy images of (a) fresh Mn/PG, (b) fresh $MnSb_{0.156}$/PG, (c) SO_2-poisoned Mn/PG and (d) SO_2-poisoned $MnSb_{0.156}$/PG. Energy-dispersive X-ray spectroscopy images of (e) fresh Mn/PG, (f) fresh $MnSb_{0.156}$/PG, (g) SO_2-poisoned Mn/PG and (h) SO_2-poisoned $MnSb_{0.156}$/PG.

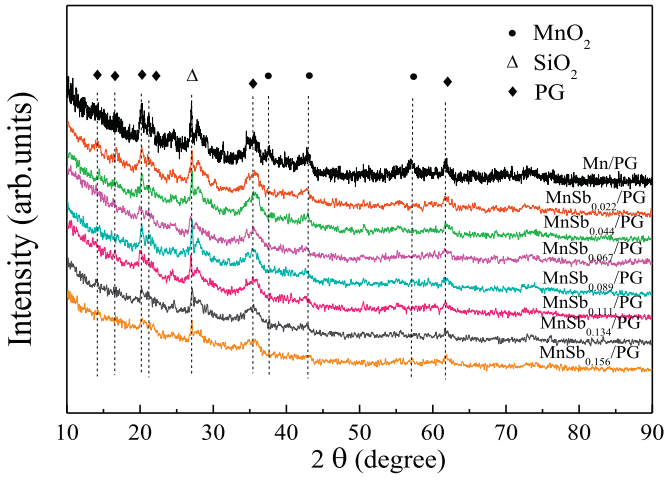

Fig. 6 – X-ray diffraction patterns of Mn/PG, $MnSb_{0.022}$/PG, $MnSb_{0.044}$/PG, $MnSb_{0.067}$/PG, $MnSb_{0.089}$/PG, $MnSb_{0.111}$/PG, $MnSb_{0.134}$/PG, and $MnSb_{0.156}$/PG.

of the peaks at 37.6°, 42.8°, 57.0° were due to the MnO_2 crystallite (PDF#30–0820). Following Sb acetate impregnation, the peaks corresponding to MnO_2 weakened in turn as Sb loading increased, which can be attributed to the amorphous phase of the formed solids. From these results pertaining to $MnSb_x$/PG, it was possible that more MnO_x (participated in SCR reaction) is dispersed in the amorphous phase in $MnSb_{0.156}$/PG, thus leading to higher activity. Besides, the amorphous structure of manganese oxide has been suggested to improve the existence of O vacancies, and enhance active component dispersion which agrees with the result of SEM analyses, leading to low sintering and high activity (Saqer et al., 2011). What's more, all these patterns did not show intense peaks of Sb compounds, indicating that Sb possibly exists in an amorphous or highly dispersed phase on the catalysts surface. Accordingly, in the case of Sb-loaded catalysts, there may be a greater contact between manganese oxides and antimony oxides, since these oxides are well dispersed on the support material.

2.2.3. *BET analyses*

The physical properties of catalysts are important in determining the adsorption-desorption phenomena of gases onto its surface. BET analysis was conducted for Mn/PG and $MnSb_{0.156}$/PG before and after SO_2 poison to understand the effect of SO_2. These SO_2 poisoned catalysts were pre-treated at 200°C for 2 hr SCR reaction in reactant gas contained NH_3, NO, O_2, Ar and 200 ppmV SO_2. The surface areas of fresh Mn/PG, SO_2-poisoned Mn/PG, fresh $MnSb_{0.156}$/PG and SO_2-poisoned $MnSb_{0.156}$/PG were 142.2, 122.1, 78.0 and 75.7 m^2/g, respectively. The surface area of the Sb-added samples is smaller than those of the raw catalysts especially for sulfated catalysts. Combined with SEM analyses, it could be deduced that the decrease in surface area for fresh Sb-added sample is ascribed to the uniform distribution of newly-formed ultramanometer material on PG surface which is growth in the structure of PG and does not influence the original microscopic of PG. For the sulfated catalysts, surface area decreased appropriate 14% on Mn/PG while just 3% decrease obtained on Sb-added catalyst compared to those of fresh samples. Since the accumulation of ammonium sulfates on catalyst surface may lead to the large decrease of catalyst surface area, it cannot be classes as the main reason for the decrease of catalyst surface area (Jin et al., 2010a). Besides, the following experiment of SO_2-TPD also confirmed the plenty existent of metal sulfates instead of ammonium sulfates especially for Mn/PG which is also in accordance with the decrease trends in catalyst's surface area. Thus, it can be deduced that there are only tiny amounts of metal sulfates produced in Sb-added catalyst and the decrease in catalyst's surface area attributes to the formation of metal sulfates rather than the decomposition ammonium sulfates.

3. Discussion

3.1. *SO_2-TPD analyses*

SO_2-TPD was performed on Mn/PG and $MnSb_{0.156}$/PG to examine the thermal stability of S contained species formed during SO_2-poisoning. As shown in Fig. 7, the desorption of SO_2 on Mn/PG began at 780°C and reached a peak at 920°C matching the pattern of decomposition of $MnSO_4$ (Yu et al., 2010; Huang et al., 2008). This result confirmed the formation of $MnSO_4$ on Mn/PG catalysts, which is considered to be the main reason for the deactivation of Mn-based catalysts (Huang et al., 2008). However, on $MnSb_{0.156}$/PG, there were two distinct peaks in the SO_2-TPD profile. One began at 550°C and peaked at 620°C and another one began at higher than 800°C as a quite weaker peak. Obviously, the second peak showed the same thermal property as that on Mn/PG which ascribes to the decomposition of $MnSO_4$. While compared to the peak on Mn/PG, this little peak is negligible. It meant that only a small amount of $MnSO_4$ is formed on the surface of $MnSb_{0.156}$/PG during SO_2-poisoning. Notably, there was a new peak appeared at lower than 800°C (peaking at about 620°C), which shows a distinctive thermal stability other than $MnSO_4$. It was more likely due to the decomposition of $Sb_2(SO_4)_3$. Thus, it was reasonable to confirm that, after the introduction of Sb, the formation of manganese sulfates is lessened. And, it could also deduce that the formation of $Sb_2(SO_4)_3$ is prior to $MnSO_4$. As discussed above, manganese oxides were proved to be the sole active specie for SCR process. Maintaining the stability of manganese active specie in the presence of SO_2 was regard to be the most important aspect for enhancing the tolerance to SO_2-poisoing for Mn based catalysts. Based on the results of SO_2-TPD, it was firmly suggested that the reaction between manganese oxides and SO_2 may be lessened by addition of Sb. Results of SEM illustrated that the morphology is changed and the dispersion of surface specie is greatly improved after Sb-loading, so that the better SCR activity can be achieved. However, the redox property of the catalyst is widely considered to be relative to the formation of surface sulfates. Therefore, more information about the change in redox property of the catalysts due to Sb addition should be presented for better comprehension.

3.2. *H_2-TPR analyses*

The redox state of $MnSb_{0.156}$/PG was investigated using H_2-TPR, and the results are shown in Fig. 8. For comparison, Mn/PG and $Sb_{0.156}$/PG were also characterised using TPR. Three main H reduction peaks with different strength were observed over Mn/PG in temperature range of 300–700°C. It was generally suggested (Ettireddy et al., 2007; Shen et al., 2014; Trawczyński et al., 2005) that the first peak at 370°C was due to the transformation of lattice O (O_β) companied with Mn to chemisorbed oxygen (O_α) (MnO_2 to Mn_2O_3), and that the peaks at 470 and 670°C could be attributed to the reductions of Mn_2O_3 to Mn_3O_4 and Mn_3O_4 to MnO, respectively. However, after Sb species incorporation into Mn/PG, the peak centred at 370°C weakened acutely, implying the markedly decrease in lattice oxygen (O_β) companied with Mn. A new peak appeared at about 600°C could be ascribed to the reduction of Sb^{5+} to Sb^{3+}, as can be confirmed from the profile of $Sb_{0.156}$/PG. The peak at 600°C for $MnSb_{0.156}$/PG was observed to be higher than for $Sb_{0.156}$/PG. It meant that part of active lattice O (O_β) companied with Mn has combined with Sb. The shift of lattice O (O_β) from Mn species to Sb species may lead to SO_2 prior reacting with Sb oxides other than Mn oxides. We calculated the area by integrating 100–800°C on the curve in the H_2-TPR

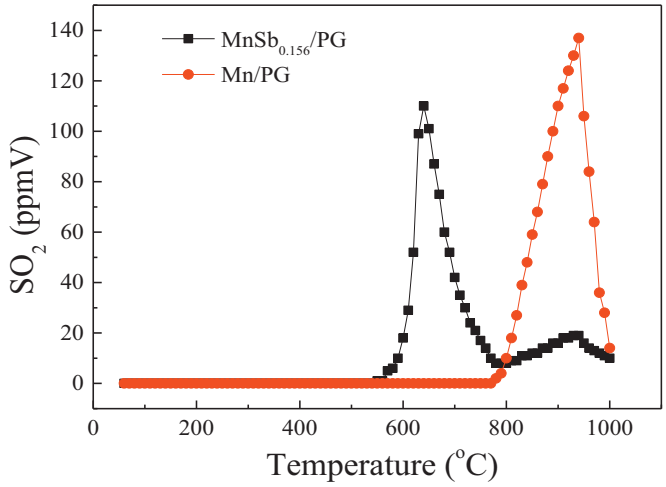

Fig. 7 – SO_2 temperature-programmed desorption patterns of Mn/PG and $MnSb_{0.156}$/PG.

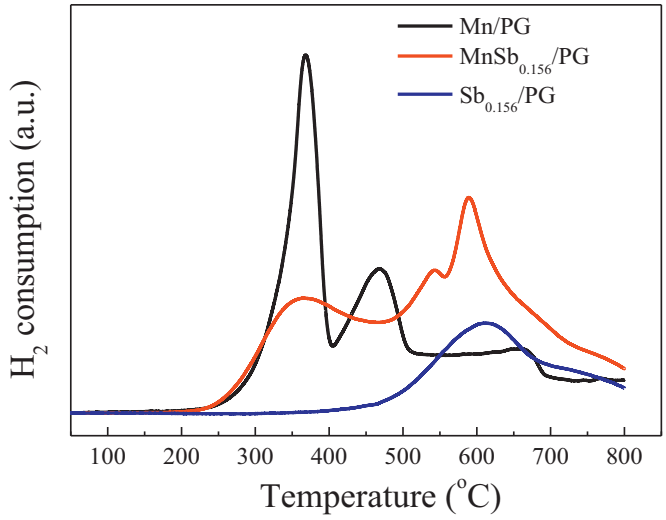

Fig. 8 – H_2-temperature-programmed reduction profiles on fresh Mn/PG, $MnSb_{0.156}$/PG and $Sb_{0.156}$/PG.

diagram. Total areas of H_2-TPR curves of Mn/PG, Sb/PG and $MnSb_{0.156}$/PG were 20,364,381, 3,843,523 and 24,288,461 a.u., respectively. The area of the $MnSb_{0.156}$/PG catalyst in the curve was about the sum of the areas of the other two samples, and its peak area of hydrogen consumption was the largest amongst the curves of three samples, indicating that the doping of Sb improved the redox performance of the manganese-based catalyst.

3.3. *XPS analyses*

Mn/PG and $MnSb_{0.156}$/PG catalysts were also characterized by XPS to identify the chemical compositions (atomic concentrations) of the surface layer and ensure the oxidation states of Mn oxides. The surface atomic concentrations of Mn, Sb, O and S from XPS are summarised in Table 1. The photoelectron spectra of Mn2p, Sb3d, O1s and S2p are displayed in Fig. 9.

Fig. 9a shows the photoelectron spectra of Mn 2p for different catalysts before and after SO_2 poisoning. The $2p_{3/2}$ binding energies at 640.3, 641.3 and 642.1 eV were attributed to the presence of surface Mn^{2+}, Mn^{3+} and Mn^{4+} species in the catalysts, respectively (Thirupathi and Smirniotis, 2011). After being pre-treated by SO_2, the primary peak of Mn $2p_{3/2}$ peak in Mn/PG was found to show a binding energy shift of −0.7 eV, which evinced that, a new surface species forms except for MnO_x. Therefore, it could be deduced that the MnO_x is sulfated during the SCR in the presence of SO_2. However, for Mn-$Sb_{0.156}$/PG, no noticeable shifts in the binding energy of Mn $2p_{3/2}$ was perceived after reactions in SO_2 containing gas, which indicates that the Sb addition can efficiently inhibit the sulfation of MnO_x on catalysts surface, shielding the active phases. In Mn/PG, the content of Mn was found to decrease sharply from 3.16% to 1.12% before and after SCR in the presence of SO_2. Besides, there was large amount of Mn^{2+} (0.23) (Table 1) existed illustrated that the presence of SO_2 may lead to an unrecoverable reaction of Mn^{2+} to Mn^{4+}/Mn^{3+} and the permanent deactivation of Mn/PG. In contrast, no obviously decrease in the content of Mn and Sb in $MnSb_{0.156}$/PG

Table 1 – X-ray photoelectron spectroscopy results of catalysts.

Catalyst	Surface atomic concentration (%)							Mn^{4+}/Mn^{3+}	Sb^{5+}/Mn^{a+}
	Mn	Mn^{2+}	S	Sb	O_T	O/O_T (%)			
						O_α/O_T	O_β/O_T		
Mn/PG	3.16	–	–	–	96.84	95.73	4.27	2.89	–
$MnSb_{0.156}$/PG	2.48	–	–	0.85	96.67	100	–	5.14	0.34
$MnSb_{0.156}$/PG-SCR	2.90	–	–	1.69	95.41	100	–	4.13	0.58
SO_2-poisoned Mn/PG	1.12	0.23	1.06	–	97.47		–	2.22	–
SO_2-poisoned $MnSb_{0.156}$/PG	2.92	–	0.36	1.14	95.58	100	–	3.93	0.39

O_β: lattice oxygen; O_α: chemisorbed oxygen; O_T: $O_\beta + O_\alpha$. Relative amounts of Mn^{4+}/Mn^{3+} are expressed in terms of atomic ratio.

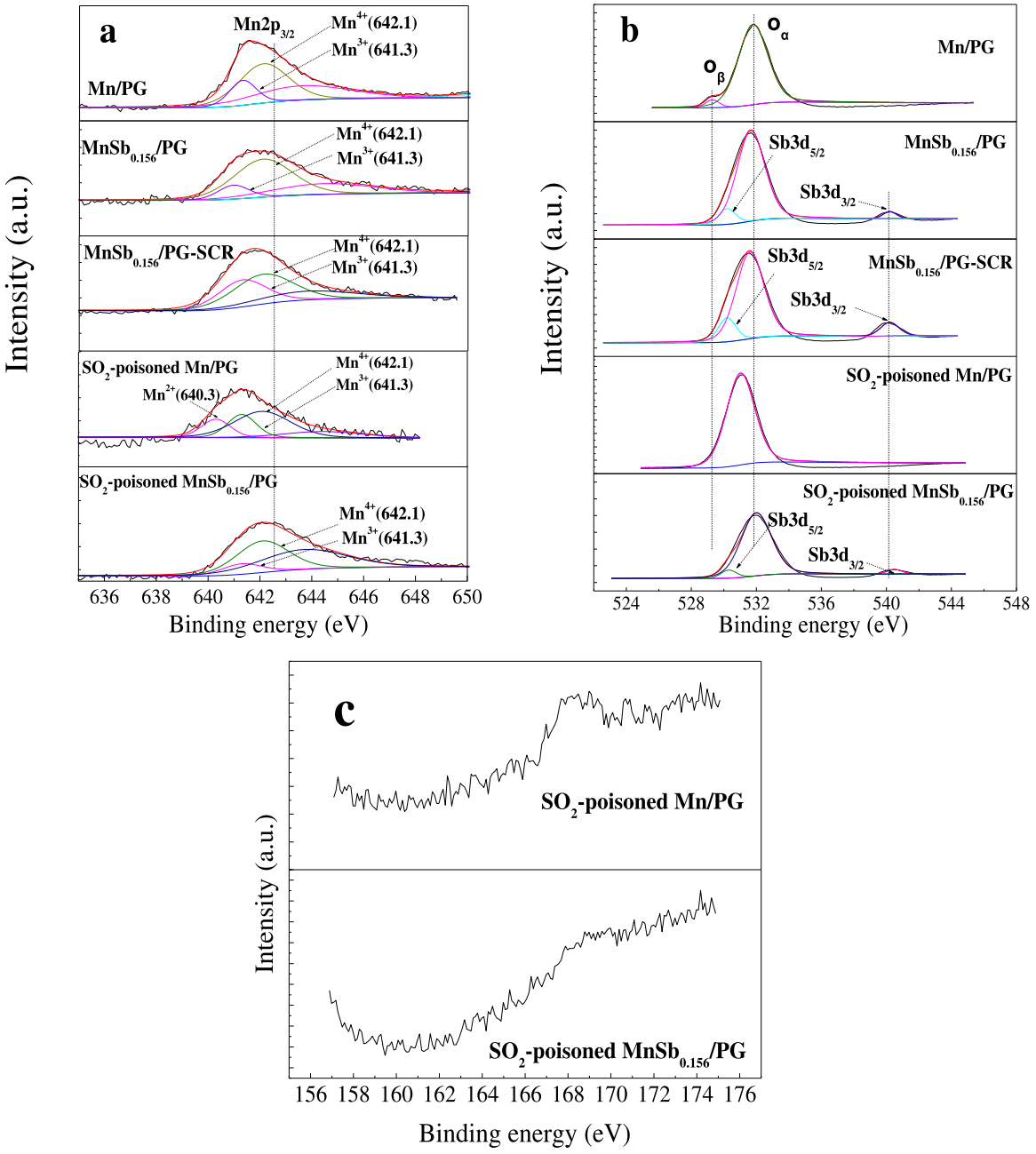

Fig. 9 – (a) Mn2p, (b) O1s and Sb3d, (c) S2p XPS spectra for five different samples.

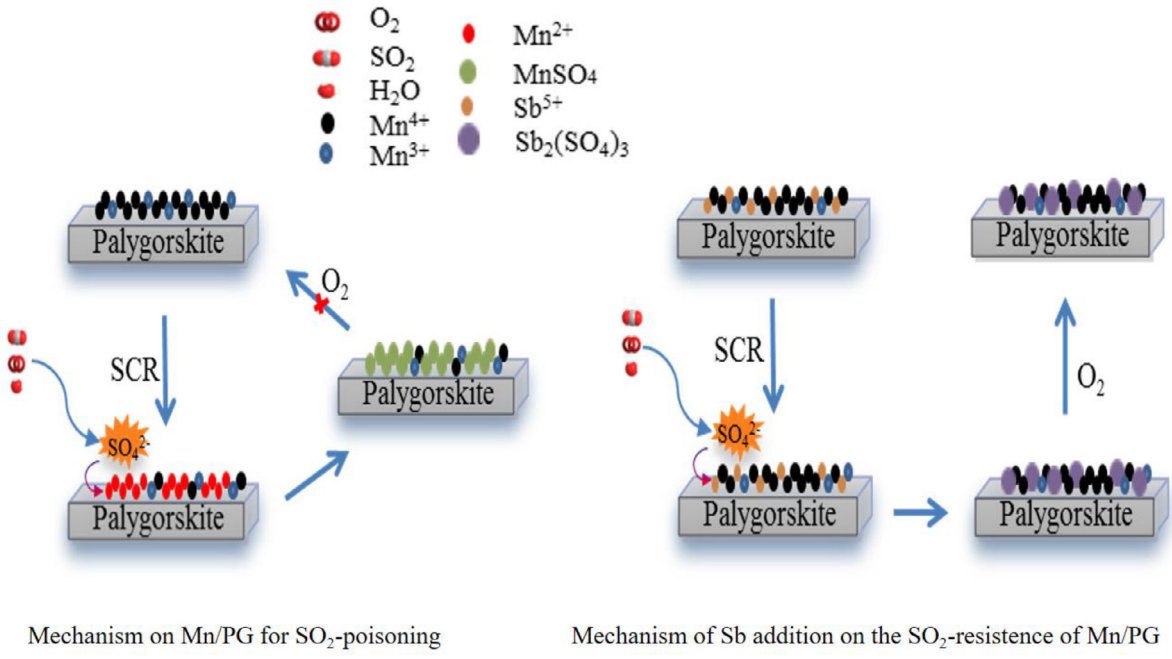

Fig. 10 – Graphical description for the effect of Sb addition on the SO_2-resistence of Mn/PG.

was found after SCR in the presence of SO_2 (Table 1), indicating that manganese oxides are ultra-highly dispersed on catalyst's surface and that MnO_x keeps stable on the surface of Sb-added catalyst. It was in accordance with the aforementioned results of SEM, XRD and H_2-TPR analyses. Furthermore, the ratios of Mn^{4+}/Mn^{3+} over the surfaces of $MnSb_{0.156}$/PG (5.14) and $MnSb_{0.156}$/PG-SCR (4.31) were relatively higher than that of the Mn/PG catalyst (2.89) (Table 1) confirmed the transition of Mn^{3+} to Mn^{4+} over the surface of PG-supported catalysts with addition of Sb oxides, which is beneficial for SCR (Kapteijn et al., 1994b). Besides, the ratio of Mn^{4+}/Mn^{3+} over the surface of SO_2-poisoned $MnSb_{0.156}$/PG (3.93) was higher than that of SO_2-poisoned Mn/PG catalyst (2.22). These results were also in accordance with the results of activity and SO_2 step-wise studies described above.

Fig. 9**b** shows the XPS spectra of O1s and Sb3d for catalysts. The XPS spectra of O1s peak for Mn/PG could be fitted into two peaks. The peak that appeared at lower binding energy (530.3–529.2 eV) could be assigned to O_β, and the additional peak that appeared at higher binding energy (532.5–531.3 eV) corresponds to the surface O_α (Guan et al., 2011). O_β transformed into O_α upon Sb oxides introduction, likely because of the oxidation of Sb^{5+} species on catalyst's surface. Surface O_α has been considered the most active O for oxidation reactions because of its higher mobility relative to O_β and is generally acknowledged to play an important role in SCR activity (Kang et al., 2007; Wu et al., 2008; Carja et al., 2007). Sb doping increases O_α on the catalyst surface and enhances SCR activity, consistent with the results shown in Fig. 1. The $Sb3d_{5/2}$ and $Sb3d_{3/2}$ spin–orbital spectrum were assigned to the binding energy at 530.2 eV and at 540.1 eV. From the Handbook of XPS (Knystautas and Singh, 1986), we can determine that the peak of $Sb3d_{5/2}$ at approximately 530.2 eV is due to Sb^{5+} species. At the same time, the peak of $Sb3d_{3/2}$ at about 540.1 eV could also be attributed to Sb^{5+} species (Montilla et al., 2004).

Fig. 9**c** represents the photoelectron spectra of S2p for Mn/PG and $MnSb_{0.156}$/PG after SO_2 poisoning. The peaks at 168.9 eV could be attributed to the S(VI), indicating the formation of sulfate species after SO_2 poisoning (Sheng et al., 2012). Combined with the result of Mn 2p spectra for SO_2 poisoned Mn/PG, it could be proved that the S element is mainly originated from $MnSO_4$. The conclusion was further confirmed by the TPD experiment for SO_2 poisoned Mn/PG. Additionally, it could also be observed that the surface S content (0.36) on SO_2-poisoned $MnSb_{0.156}$/PG is lower than that of SO_2-poisoned Mn/PG (1.06) (Table 1), which suggests that the generation of sulfate species on catalyst surface is inhibited after Sb doping. Combined with experiment of TPD, the possible reason is that Sb dopants would preferentially react with SO_2 to form $Sb_2(SO_4)_3$ and thereby shields the active MnO_x phases from being sulfated.

3.4. *Mechanism*

A similar mechanism for SCR over manganese based catalysts has generally been proposed by many researchers based on Eley-Rideal route in the past decades (Kijlstra et al., 1997a, 1997b). Manganese based catalysts are proved to have high SCR activity and selectivity at low temperatures. Adsorption and following middle oxidation of NH_3 are believed to be the key step of SCR process over manganese based catalysts just as over vanadium based catalyst which has been commercialized for decades (Topsoe et al., 1995a, 1995b; Kapteijn et al., 1994a). The redox cycle of manganese oxides helped to moderately oxidize adsorbed NH_3 rather than excessively oxidize ammonia to produce many side reaction (Liu et al., 2014). How-

ever, when exposed to a SO_2 containing flue gas, the manganese based catalysts often suffer from serious deactivation (Jin et al., 2014). So many attempts are applied to enhancing the SO_2 tolerance including optimization of preparation, nanolization of carrier and modification by additives (Wang et al., 2013; Thirupathi and Smirniotis, 2011; Guan et al., 2011). amongst various elements, rare-earth metals are most often used as additives for their good property as lattice oxygen reservoir (Jiang et al., 2014). While, prior to developing an effective method for improving SO_2 tolerance on manganese based catalysts, a comprehensive understanding on the deactivation of the catalysts caused by SO_2 is essential. In this paper, we found that the modification of Sb as additive on Mn/PG catalyst remarkably improved tolerance to SO_2-poisoning.

According to the discussion above, a reasonable mechanism about the promotion on the SO_2 tolerance of $MnSb_{0.156}$/PG as well as the deactivation of Mn/PG caused by SO_2 can be proposed, as illustrated in Fig. 10.

Firstly, the deactivation route for Mn/PG is described in Fig. 10a. It was proved that the sulfation of manganese oxides other than the deposition of ammonium sulfates mainly caused the permanent deactivation of the catalyst. Gaseous SO_2 was firstly oxidized by the active lattice oxygen which combines with Mn species, and consequently reacted with Mn to form $MnSO_4$ with high thermal stability. In this way, the redox cycle of MnO_x was interrupted. As a result, the continuous middle oxidation of adsorbed NH_3 depending on this redox cycle was also inhibited. In one word, the generation of $MnSO_4$ reduced the number of active sites of MnO_x and led to an unrecovered reaction of Mn^{2+} to Mn^{4+}/Mn^{3+}.

For $MnSb_{0.156}$/PG catalyst, as discussed in H_2-TPR and XPS analyses, quite a part of lattice oxygen initially combined with Mn was shifted to Sb sites. The oxidation of SO_2 to SO_3 was then occurred at the site of Sb owing to the shift of lattice oxygen. On the other side, due to the decrease of lattice oxygen combined with Mn, the in-situ oxidation of SO_2 to SO_3 on the site of Mn was diminished, so did the formation of manganese sulfates. Thus, the redox cycle of MnO_x for SCR was continuously maintained.

4. Conclusions

Manganese oxides supported palygorskite (Mn/PG) catalyst has been proved to be reliable for SCR at lower temperatures. While it often suffered from a serious deactivation when exploded to gases contained SO_2, preventing it from practical application for industrial flue gas NO removal at lower temperatures. For the sake of promoting the performance of Mn/PG catalyst for SCR in presence of SO_2, namely SO_2 tolerance, functional additive Sb was doped to obtain a modified catalyst $MnSb_x$/PG. The catalytic activity of the catalyst was found to be remarkably improved by the addition of Sb either or not in the presence of SO_2. $MnSb_{0.156}$/PG catalyst displays higher durable resistance to SO_2 than the Mn/PG catalyst does. Despite of mild accumulation in deposition of ammonium sulfates, the fundamental inhibition of manganese sulfates formation was found to be the key reason for great enhancement in SO_2 tolerance of the catalysts after Sb addition. SEM and XRD results showed that due to Sb loading, originally formed MnO_x crystallite has been completely transformed into highly dispersed amorphous phase. According to the results of SO_2-TPD, H_2-TPR and XPS analyses, a mechanism about the deactivation of Mn/PG caused by SO_2 and the promotion on SO_2 tolerance of $MnSb_{0.156}$/PG can be proposed as following. For Mn/PG, gaseous SO_2 was firstly oxidized by the active lattice oxygen combined with Mn species, and consequently reacted with Mn to form $MnSO_4$ which interrupts the redox cycle of MnO_x caused the permanent deactivation. In different, for Sb-doped Mn/PG catalyst, due to the shift of lattice oxygen from Mn sites to Sb sites, the in-situ oxidation of SO_2 to SO_3 on Mn sides was diminished, so did the formation of manganese sulfates. Thus, the redox cycle of MnO_x for SCR was continuously maintained.

Acknowledgments

This work was supported by the National Natural Science Foundation of China (No. 51872070).

REFERENCES

Aguero, F.N., Barbero, B.P., Gambaro, L., Cadus, L.E., 2009. Catalytic combustion of volatile organic compounds in binary mixtures over MnO_x/Al_2O_3 catalyst. Appl. Catal. B-Environ. 91, 108–112.

Amiridis, M.D., Duevel, R.V., Wachs, I.E., 1999. The effect of metal oxide additives on the activity of V_2O_5/TiO_2 catalysts for the selective catalytic reduction of nitric oxide by ammonia. Appl. Catal. B-Environ. 20, 111–122.

Biervliet, M., Poels, E.K., Bliek, A., 1998. Deactivation by SO_2 of MnO_x/Al_2O_3 catalysts used for the selective catalytic reduction of NO with NH_3 at low temperatures. Appl. Catal. B-Environ. 16, 327–337.

Burkardt, A., Weisweiler, W., 2001. Influence of the V_2O_5 loading on the structure and activity of V_2O_5/TiO_2 SCR catalysts for vehicle application. Top. Catal. 16, 369–375.

Busca, G., Lietti, L., Ramis, G., Berti, F., 1998. Chemical and mechanistic aspects of the selective catalytic reduction of NO_x by ammonia over oxide catalysts: a review. Appl. Catal. B-Environ. 18, 1–36.

Carja, G., Kameshima, Y., Okada, K., Madhusoodana, C.D., 2007. Synthesis and characterization of mesoporous silica from selectively acid-treated saponite as the precursors. Appl. Catal. B-Environ. 73, 60–64.

Colombo, M., Nova, I., Tronconi, E., 2010. A comparative study of the NH_3-SCR reactions over a Cu–zeolite and a Fe–zeolite catalyst. Catal. Today 151, 223–230.

Du, X., Gao, X., Fu, Y., Gao, F., Luo, Z., 2012. The co-effect of Sb and Nb on the SCR performance of the V_2O_5/TiO_2 catalyst. J. Colloid Interface Sci. 368, 406–412.

Ettireddy, P.R., Ettireddy, N., Mamedov, S., Boolch, P., Smirniotis, P.G., 2007. Surface characterization studies of TiO_2 supported manganese oxide catalysts for low temperature SCR of NO with NH_3. Appl. Catal. B-Environ. 76, 123–134.

Forzatti, P., 2001. Present status and perspectives in de-NO_x SCR catalysis. Appl. Catal. A-Gen. 222, 221–236.

Guan, B., Lin, H., Zhu, L., Huang, Z., 2011. Selective catalytic reduction of NO_x with NH_3 over Mn, Ce substitution $Ti_{0.9}V_{0.1}O_{2-\delta}$ nanocomposites catalysts prepared by self-propagating high-temperature synthesis method. J. Phys. Chem. C 115, 12850–12863.

Guo, R.T., Pan, W.G., Yang, N.Z., Chen, Q.L., 2016. The promotion effect of Sb on the Na resistance of Mn/TiO_2 catalyst for selective catalytic reduction of NO with NH_3. Fuel 169, 87–92.
Guo, R.T., Sun, X., Liu, J., Pan, W.G., 2018. Enhancement of the NH_3-SCR catalytic activity of $MnTiO_x$ catalyst by the introduction of Sb. Appl. Catal. A-Gen. 558, 1–8.
Huang, J., Tong, Z., Huang, Y., Zhang, J., 2008. Sulfur poisoning resistant mesoporous Mn-base catalyst for low-temperature SCR of NO with NH_3. Appl. Catal. B-Environ. 78, 309–314.
Huang, Z., Zhu, Z., Liu, Z., Liu, Q., 2003. Formation and reaction of ammonium sulfate salts on V_2O_5/AC catalyst during selective catalytic reduction of nitric oxide by ammonia at low temperatures. J. Catal. 214, 213–219.
Jiang, H.X., Zhao, J., Jiang, D.Y., Zhang, M.H., 2014. Hollow MnO_x–CeO_2 nanospheres prepared by a green route: a novel low-temperature NH_3-SCR catalyst. Catal. Lett. 144, 325–332.
Jin, R., Liu, Y., Wang, Y., Cen, W., Wu, Z., Wang, H., et al., 2014. The role of cerium in the improved SO_2 tolerance for NO reduction with NH_3 over Mn-Ce/TiO_2 catalyst at low temperature. Appl. Catal. B-Environ. 148, 582–588.
Jin, R., Liu, Y., Wu, Z., Wang, H., Gu, T., 2010a. Relationship between SO_2 poisoning effects and reaction temperature for selective catalytic reduction of NO over Mn–Ce/TiO_2 catalyst. Catal. Today 153, 84–89.
Jin, R.B., Liu, Y., Wu, Z.B., Wang, H.Q., Gu, T.T., 2010b. Low-temperature selective catalytic reduction of NO with NH3 over MnCe oxides supported on TiO_2 and Al_2O_3: a comparative study. Chemosphere 78, 1160–1166.
Kang, M., Park, E.D., Kim, J.M., Yie, J.E., 2007. Manganese oxide catalysts for NO_x reduction with NH_3 at low temperatures. Appl. Catal. A-Gen. 327, 261–269.
Kapteijn, F., Singoredjo, L., Andreini, A., Moulijn, J.A., 1994a. Activity and selectivity of pure manganese oxides in the selective catalytic reduction of nitric oxide with ammonia. Appl. Catal. B-Environ. 3, 173–189.
Kapteijn, F., Vanlangeveld, A.D., Moulijn, J.A., Andreini, A., Vuurman, M.A., 1994b. Alumina-supported manganese oxide catalysts: I. characterization: effect of precursor and loading. J. Catal 150, 94–104.
Karami, A., Salehi, V., 2012. The influence of chromium substitution on an iron–titanium catalyst used in the selective catalytic reduction of NO. J. Catal. 292, 32–43.
Kijlstra, W.S., Brands, D.S., Poels, E.K., Bliek, A., 1997a. Mechanism of the selective catalytic reduction of NO by NH3 over MnO_x/Al_2O_3 .1. adsorption and desorption of the single reaction components. J. Catal. 171, 208–218.
Kijlstra, W.S., Brands, D.S., Poels, E.K., Bliek, A., 1997b. Mechanism of the selective catalytic reduction of NO with NH3 over MnO_x/Al_2O_3. J. Catal. 171, 219–230.
Kim, Y.J., Kwon, H.J., Nam, I.S., Choung, J.W., Kil, J.K., Yeo, G.K., 2010. High deNO_x performance of Mn/TiO_2 catalyst by NH_3. Catal. Today 151, 244–250.
Knystautas, E.J., Singh, A., 1986. X-ray photoelectron spectroscopy of boron implanted 4145 steel surface. Appl. Phys. A 40, 91–93.
Kobayashi, M., Hagi, M., 2006. Low temperature selective catalytic reduction of NO by NH_3 over V_2O_5 supported on TiO_2-SiO_2-MoO_3. Appl. Catal. B-Environ. 63, 104–113.
Li, X., Zhang, S., Jia, Y., Liu, X., Zhong, Q., 2012. Selective catalytic oxidation of NO with O_2 over Ce-doped MnO_x/TiO_2 catalysts. J. Nat. Gas Chem. 21, 17–24.
Liu, Z., Zhu, J., Li, J., Ma, L., Woo, S.I., 2014. Novel CO_2-capture derived from the basic ionic liquids orientated on mesoporous materials. ACS Appl. Mater. Inter. 6, 14500–14508.
Lu, X., Song, C., Chang, C.C., Teng, Y., Tong, Z., Tang, X., 2014. Manganese oxides supported on TiO_2–graphene nanocomposite catalysts for selective catalytic reduction of NO_x with NH_3 at low temperature. J. Ind. Eng. Chem. 53, 11601–11610.
Marbán, G., Fuertes, A.B., 2001. Low-temperature SCR of NO_x with NH_3 over Nomex™ rejects-based activated carbon fibre composite-supported manganese oxides: part II. effect of procedures for impregnation and active phase formation. Appl. Catal. B-Environ. 34, 55–71.
Middea, A., Spinelli, L.S., Neumann, R., 2015. Synthesis and characterization of magnetic palygorskite nanoparticles and their application on methylene blue remotion from water. Appl. Surf. Sci. 346, 232–239.
Montilla, F., Morallón, E., Battisti, A.D., Barison, S., 2004. Preparation and characterization of antimony-doped tin dioxide electrodes. 3. XPS and SIMS characterization. J. Phys. Chem. B 108, 15976–15981.
Park, T.S., Jeong, S.K., Hong, S.H., Hong, S.C., 2001. A highly distributed Cu_xAu_y-deposited nanotube carbon for selective reduction of NO in the presence of NH_3 at very low temperature. J. Ind. Eng. Chem. 40, 4491–4495.
Park, E., Kim, M., Jung, H., Chin, S., Jurng, J., 2013. Effect of sulfur on Mn/Ti catalysts prepared using chemical vapor condensation (CVC) for low-temperature NO reduction. ACS Catal. 3, 1518–1525.
Peña, D.A., Uphade, B.S., Smirniotis, P.G., 2004. TiO_2-supported metal oxide catalysts for low-temperature selective catalytic reduction of NO with NH_3: I. evaluation and characterization of first row transition metals. J. Catal. 221, 421–431.
Phil, H.H., Reddy, M.P., Kumar, P.A., 2008. SO_2 resistant antimony promoted V_2O_5/TiO_2 catalyst for NH_3-SCR of NO_x at low temperatures. Appl. Catal. B-Environ. 78, 301–308.
Qi, G., Yang, R.T., 2003. Low-temperature selective catalytic reduction of NO with NH_3 over iron and manganese oxides supported on titania. Appl. Catal. B-Environ. 44, 217–225.
Rauch, D., Albrecht, G., Kubinski, D., Moos, R., 2015. A microwave-based method to monitor the ammonia loading of a vanadia-based SCR catalyst. Appl. Catal. B-Environ. 165, 36–42.
Saqer, S.M., Kondarides, D.I., Verykios, X.E., 2011. Catalytic oxidation of toluene over binary mixtures of copper, manganese and cerium oxides supported on γ-Al_2O_3. Appl. Catal. B-Environ. 103, 275–286.
Schneider, H., Maciejewski, M., Kohler, K., Wokaun, A., Baiker, A., 1995. Chromia supported on titania: VI. properties of different chromium oxide phases in the catalytic reduction of NO by NH_3 studied by in situ diffuse reflectance FTIR spectroscopy. J. Catal. 157, 312–320.
Schuler, A., Votsmeier, M., Kiwic, P., Gieshoff, J., Hautpmann, W., Drochner, A., et al., 2009. NH_3-SCR on Fe zeolite catalysts - from model setup to NH_3 dosing. Chem. Eng. J. 154, 333–340.
Shen, B.X., Wang, Y.Y., Wang, F.M., Liu, T., 2014. The effect of Ce–Zr on NH_3-SCR activity over $MnO_x(0.6)/Ce_{0.5}Zr_{0.5}O_2$ at low temperature. Chem. Eng. J. 236, 171–180.
Sheng, Z., Hu, Y., Xue, J., Wang, X., Liao, W., 2012. SO_2 poisoning and regeneration of Mn-Ce/TiO_2 catalyst for low temperature NO_x reduction with NH_3. J. Rare Earth 30, 676–682.
Shi, Y.N., Chen, S., Sun, H., Shu, Y., Quan, X., 2013. Low-temperature selective catalytic reduction of NO_x with NH_3 over hierarchically macro-mesoporous Mn/TiO_2. Catal. Commun. 42, 10–13.
Shu, Y., Aikebaier, T., Quan, X., Chen, S., Yu, H., 2014. Selective catalytic reaction of NO_x with NH_3 over Ce–Fe/TiO_2-loaded wire-mesh honeycomb: resistance to SO_2 poisoning. Appl. Catal. B-Environ. 150, 630–635.
Sreekanth, P.M., Peña, D.A., Smirniotis, P.G., 2006. Titania supported bimetallic transition metal oxides for low-temperature SCR of NO with NH_3. J. Ind. Eng. Chem. 45, 6444–6449.
Sun, Z.M., Yu, Y.C., Pang, S.Y., Du, D.Y., 2013. Manganese-modified activated carbon fiber (Mn-ACF): novel efficient adsorbent for arsenic. Appl. Surf. Sci. 284, 100–106.

Thirupathi, B., Smirniotis, P.G., 2011. Co-doping a metal (Cr, Fe, Co, Ni, Cu, Zn, Ce, and Zr) on Mn/TiO_2 catalyst and its effect on the selective reduction of NO with NH_3 at low-temperatures. Appl. Catal. B-Environ. 110, 195–206.

Topsøe, N.Y., 1994. Mechanism of the selective catalytic reduction of nitric oxide by ammonia elucidated by in situ on-line Fourier transform infrared spectroscopy. Science 265, 1217–1219.

Topsoe, N.Y., Dumesic, J.A., Topsoe, H., 1995a. Vanadia-titania catalysts for selective catalytic reduction of nitric-oxide by ammonia: I.I. studies of active sites and formulation of catalytic cycles. J. Catal. 151, 241–252.

Topsoe, N., Topsoe, H., Dumesic, J., 1995b. Vanadia/titania catalysts for selective catalytic reduction (SCR) of nitric-oxide by ammonia: I. combined temperature-programmed in-situ FTIR and on-line mass-spectroscopy studies. J. Catal. 151, 226–240.

Trawczyński, J., Bielak, B., Miśta, W., 2005. Oxidation of ethanol over supported manganese catalysts—Effect of the carrier. Appl. Catal. B-Environ. 55, 277–285.

Wang, X., Zheng, Y.Y., Xu, Z., Wang, X.L., Chen, X.P., 2013. Amorphous MnO_2 supported on carbon nanotubes as a superior catalyst for low temperature NO reduction with NH_3. RSC Adv. 3, 11539–11542.

Wu, Z.B., Jin, R.B., Liu, Y., Wang, H.Q., 2008. Ceria modified MnO_x/TiO_2 as a superior catalyst for NO reduction with NH_3 at low-temperature. Catal. Commun. 9, 2217–2220.

Wu, Z.B., Jin, R.B., Wang, H.Q., Liu, Y., 2009. Effect of ceria doping on SO_2 resistance of Mn/TiO_2 for selective catalytic reduction of NO with NH_3 at low temperature. Catal. Commun. 10, 935–939.

Yu, J., Guo, F., Wang, Y., Zhu, J., Liu, Y., Su, F., et al., 2010. Sulfur poisoning resistant mesoporous Mn-base catalyst for low-temperature SCR of NO with NH_3. Appl. Catal. B-Environ. 95, 160–168.

Zhang, J., Huang, Y., Chen, X., 2008. Selective catalytic oxidation of NO over iron and manganese oxides supported on mesoporous silica. J. Nat. Gas Chem. 17, 273–277.

Zhang, X.L., Lv, S.S., Zhang, C.P., Wu, X.P., 2015. Effect of SO_2 on SCR activity of MnO_x/PG catalysts at low temperature. Chem. Papers 69, 1548–1555.

Zhang, D.S., Zhang, L., Fang, C., Gao, R.H., Qian, Y.L., 2013. MnO_x–CeO_x/CNTs pyridine-thermally prepared via a novel in situ deposition strategy for selective catalytic reduction of NO with NH_3. RSC Adv. 3, 8811–8819.

Zhang, Y.P., Zhao, X.Y., Xu, H.T., Shen, K., Zhou, C.C., Jin, B.S., et al., 2011. Novel ultrasonic–modified MnO_x/TiO_2 for low-temperature selective catalytic reduction (SCR) of NO with ammonia. J. Colloid Interface Sci. 361, 2212–2218.